JCTC Journal of Chemical Theory and Computation

Reduced Catalytic Activity of P450 2A6 Mutants with Coumarin: A Computational Investigation

Weihua Li,[†,‡] Hirotaka Ode,[†] Tyuji Hoshino,*[,†] Hong Liu,[§] Yun Tang,*[,‡] and Hualiang Jiang[‡,§]

Graduate School of Pharmaceutical Sciences, Chiba University, Chiba 263-8522, Japan, School of Pharmacy, East China University of Science and Technology, Shanghai 200237, China, and Shanghai Institute of Materia Medica, Chinese Academy of Sciences, Shanghai 201203, China

Received January 11, 2009

Abstract: Human cytochrome P450 2A6 is the major enzyme to catalyze coumarin 7-hydroxylation, and this enzyme also plays an important role in the metabolism of nicotine and other tobacco-specific compounds. Recent experimental data showed that the N297S and A481T mutants of P450 2A6 decreased the catalytic activity toward coumarin by about 4-fold and 10-fold, respectively. These two mutants also had about 30-fold decrease in binding affinity for coumarin when compared to its wild type. At present, however, how the mutations affect the enzymatic activity and/or the substrate binding remains unclear. In this study, a combination of molecular docking and molecular dynamics (MD) simulation was employed to investigate the above question. Our results demonstrated that the N297S mutation altered the hydrogen-bonding network mediated by a water molecule between the B′−C loop and the I helix and thus a shift of the B′ helix/B′−C loop region, whereas the A481T mutation triggered the conformational changes of its adjacent residues including Phe209 and Phe280 via an indirect manner to affect the substrate binding. However, the mutations did not significantly alter the substrate binding orientation because the only polar residue 297 in the active site provided the hydrogen-bonding donor to guide the binding of coumarin. Both mutations perturbed the shape of "Phe-cluster" in the active site and thus weakened the interactions with coumarin. The calculated binding free energies were in agreement with the relative potency of the experimental binding affinities.

1. Introduction

Cytochromes P450 (CYPs) are a superfamily of heme-containing monooxygenases. These enzymes play key roles not only in the metabolism and detoxification of a large number of xenobiotic chemicals but also in the biosynthesis of many endogenous compounds.[1] Cytochrome P450 2A6 (CYP2A6) is one of the 57 CYP isoenzymes found in humans, which exists mainly in the liver and is also expressed in extrahepatic tissues.[2]

CYP2A6 can specifically catalyze coumarin 7-hydroxylation,[3] which has been used as an isoform-specific marker reaction for estimating individual's CYP2A6 activity in vivo.[4] Another important aspect of CYP2A6 is its role in the metabolism and activation of some carcinogenic compounds. For example, it was shown to be one of the major enzymes responsible for nicotine metabolism.[5] In addition to nicotine, CYP2A6 also catalyzes activation of many tobacco-specific nitrosamines and other toxic compounds, including NNN (*N*′-nitrosonicotine),[7] NNK (4-(methylnitrosamino)-1-(3-pyridy)-1-butanone),[6,7] and MTBE (methyl *t*-butyl ether).[8] For this reason, CYP2A6 has been proposed to be a potential drug target for

* Corresponding author phone: +81-43-2902926; fax: +81-43-2902925; e-mail: hoshi@p.chiba-u.ac.jp (T.H.), phone: +86-21-64251052; fax: +86-21-64253651; e-mail: ytang234@ecust.edu.cn (Y.T.).

† Chiba University.

‡ East China University of Science and Technology.

§ Chinese Academy of Sciences.

10.1021/ct900018t CCC: $40.75
Published on Web 03/30/2009

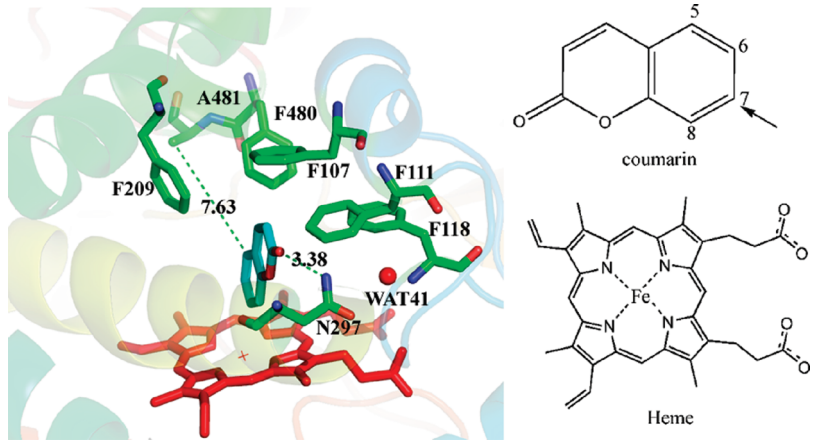

Figure 1. A close view of coumarin bound in the active site of CYP2A6 (PDB code 1Z10). Asn297, Ala481 and the Phe-cluster are labeled. The distances (Å) between coumain and Asn297 as well as Ala481 are labeled. The water molecule mediated between N297 and the B′−C loop is shown in red sphere. The 2D structures of coumarin and heme are shown on the right side. The arrow indicates the oxidation site of coumarin by CYP2A6.

smoking cessation.[9] Like other CYPs, CYP2A6 also contributes to the metabolism of several drugs, such as tegafur[10] and losigamone.[11] In addition, CYP2A6 is a genetically polymorphic enzyme.[12] More than 30 CYP2A6 variant alleles have been identified so far (http://www.imm.ki.se/CYPalleles/cyp2a6.htm).

Furthermore, CYP2A6 has indicated its potential application in the pharmaceutical industry. Work from Guengerich group demonstrated that CYP2A6 was a good biocatalyst to catalyze the oxidation of indoles to indigo and indirubin.[13] Subsequent studies from the same group found that some CYP2A6 mutants were more active than its wild type (WT) in forming indigo.[14] Several CYP2A6 mutant enzymes generated with a randomized library approach showed high inhibitory activity against human cyclin-dependent kinases (CDK)-1 and -5 and glycogen synthase kinase-3 (GSK3), two important drug targets related to a variety of diseases, for instance, cancer.[15]

Recently, Kim et al.[16] discovered several CYP2A6 mutants exhibiting altered catalytic activities with coumarin by using a combination technique of random mutagenesis and high-throughput screening. Their results demonstrated that CYP2A6 N297S and A481T mutants decreased catalytic efficiency (K_{cat}/K_m) toward coumarin by 4 and 10 times or so, respectively. These two mutants also had about 30-fold decrease in binding affinity for coumarin when compared to WT. They suggested that the reduced binding affinity was a major basis for the decreased catalytic efficiency.[16] The crystal structure of WT CYP2A6 in complex with coumarin was determined recently,[17] which provides useful static structural information on the active site. The structure reveals that coumarin is confined within the active site consisting of a "Phe-cluster" formed by residues Phe107, Phe111, Phe108, Phe209, and Phe480, as shown in Figure 1. Residue Asn297 functions as a hydrogen-bonding donor to interact with coumarin directly (Figure 1). Accordingly, it was generally believed that replacement of Asn297 by other residues might change the direct interaction between the residue 297 and coumarin.[16,18] However, when Asn297 is substituted with serine, the direct hydrogen-bonding interaction may still exist because the hydroxyl group of serine is also able to serve as a hydrogen-bonding donor. Hence, how the N297S mutation decreases the binding affinity of CYP2A6 with coumarin is poorly understood. As for Ala481, the crystal structure shows that this residue is about 7.6 Å away from the substrate and does not directly interact with the substrate (Figure 1). Therefore, it also remains unclear how the A481T mutation affects the substrate binding.

In the present work, to elucidate the mechanism underlying the reduced catalytic activity of CYP2A6 for coumarin due to residual mutation, molecular docking combined with molecular dynamic simulations and binding free-energy calculations was performed on the WT and mutant systems. Our results indicate that both N297S and A481T mutations trigger the conformation changes of the Phe-cluster and thus alter the shape of the active site of the enzymes. These alterations weaken the interactions of the substrate with the mutated enzymes. The calculated binding free energies are in agreement with the relative potency of coumarin bound with CYP2A6 WT and the mutants.

2. Methods

2.1. Construction of N297S and A481T Models. To date, several CYP2A6 crystal structures including different ligand-free mutants and ligand-bound complexes have been determined, but there is only one crystal structure available for CYP2A6 in complex with coumarin (PDB code 1Z10, at 1.9 Å resolution).[17] Therefore, for consistency, the protein models of the substrate-free N297S and A481T mutants were constructed based on the available 2A6 WT-coumarin crystal structure. The mutations at positions 297 and 481 were accomplished by *Sybyl7.0* (Tripos Inc.). The resulting mutant N297S and A481T models were subjected to energy-minimization. The detailed protocol for the minimization was described in the subsequent MD simulations section. After the minimization, the mutant models were refined by 1.0 ns MD simulations with position restraints on the protein backbone atoms excluding the residues within 5.0 Å around the mutated residues.

2.2. Molecular Docking. The substrate, coumarin, was docked into the active sites of the MD-refined CYP2A6

N297S and A481T mutants using *GOLD* version 3.2.[19] The Chemscore scoring function with specific parameters[20] for heme-containing proteins was used to rank the docking poses. This scoring function has been validated to outperform the Goldscore scoring function when applied to CYP docking by previous studies.[20,21] The Fe atom of the heme group was chosen as the center for docking and the residues within 20.0 Å around this atom were defined as the binding site. Twenty solutions were output for each docking and ranked according to Chemscore. The pose with lowest Chemscore was selected as the initial conformation for the further long-time MD simulation.

2.3. Parameterization of Heme−Thiolate Complex and Coumarin. To derive appropriate force field parameters for heme group used for molecular dynamics simulations, quantum chemical calculation was performed on the heme−thiolate complex. According to the generalized catalytic cycle of P450[22] and the crystal structure of CYP2A6-coumarin,[17] binding of the substrate displaced the water molecule that is coordinated to iron and led to a low to high spin conversion of heme. Therefore, we model the heme−thiolate complex in its pentacoordinate ferric form with the sextet spin state. The fifth coordination of iron was treated as S−Cys, and the acetyl (ACE) and *N*-methyl (NME) groups as the capping residues for Cys439. The geometrical optimization of heme-thiolate complex was performed at HF/6-31G* level. Subsequently, population analysis was carried out with the B3LYP method.[23,24] For the Fe atom, the triple-ζ-valence (TZV) basis set was used, and for H, C, N, O, and S atoms, the 6-31G* basis set was employed. On the basis of the calculated electron population, atomic charges were derived using restrained electrostatic potential (RESP) fitting procedure,[25] which ensures that the derived atom charges are compatible with the standard AMBER force field. For the force constant parameters involving Fe, we adopted the values that were kindly provided by Dr. Harris from his previous work.[26]

Atom charges of coumarin were obtained using the similar procedure as above. Geometrical optimization and the electrostatic potential were executed at the B3LYP/6-31G** level. The RESP procedure implemented in the *Amber9* antechamber module was utilized to derive the partial atomic charges of coumarin. All quantum chemical calculations were executed using the *Gaussian03* program.[27]

2.4. Protein Preparation for MD Simulations. The initial structural model of CYP2A6 WT complexed with coumarin for MD simulation was taken from the Protein Data Bank (PDB entry code 1Z10).[17] The PDB file of 1Z10 contains 4 asymmetric 2A6 molecules. Molecule A was used to present the results of the modeling and MD simulations in this study. For verification of the results, molecule B also was repeated to perform the same modeling and simulations as molecule A. Therefore, a total of 12 MD simulations were performed in this study. Six MD simulations (3 position-restrained simulations for substrate-free systems of WT, N297S and A481T, each by 1 ns; 3 unrestrained simulations for substrate-bound complexes of WT, N297S and A481T, each by 6 ns) were done for molecule A of 1Z10. Likewise, 6 MD simulations were carried out for molecule B of 1Z10 for the purpose of validation of our conclusion. It should be noted that Leu370 in molecule A has a split conformation. For consistency with molecule B, the conformation with the side chain pointing to coumarin was used for Leu370 in this study. The protonation states of charged residues and histidines were determined on the basis of pK_a values calculated by *PROPKA*.[28] According to the calculation results, His229 and His254 were assigned to be fully protonated at both nitrogen atoms. His72 and His477 were assigned to be protonated at ε nitrogen and other histidines to be protonated at δ nitrogen atoms. In addition, Glu448 was set in the protonated state (pK_a = 8.24).

An all-atom model of CYP2A6 WT was generated using the xleap module in *Amber9*.[29] All crystallization water molecules were kept in the initial model. The initial models of 2A6 N297S and A481T mutants complexed with coumarin for MD simulations were obtained from the docking results. Because only a few residues in the active site underwent the conformational changes in the two mutant models, the coordinates of all crystallization water molecules were copied into the mutant models from 1Z10 to keep as consistent with WT as possible in the initial states. The resulted models were then solvated with water molecules in a truncated octahedron periodic box. The distance between the box walls and the protein was set to 10.0 Å, which resulted in about 13 000 water molecules for each system. The TIP3P[30] water model was used. The systems were neutralized by adding the corresponding number of counterions.

2.5. MD Simulations. All of the MD simulations were performed using the *Amber9* package.[29] The AMBER ff03 all atom force field[31] was used for the protein and the general AMBER force field[32] was used as the parameters for coumarin. Energy minimization was conducted in three steps. First, only water molecules and ions were allowed to move. Next, the movement was extended to the residues within 5.0 Å around the mutated residue and the substrate (if any). Finally, all atoms were allowed to move freely. In each step, energy minimization was carried out by a combination of the steepest descent method for 5000 steps and the conjugated gradient method for another 5000 steps. After the minimization, each system was gradually heated from 0 to 300 K over 60 ps under the NVT ensemble condition and equilibrated at 300 K for 100 ps. Finally, 6.0 ns unrestrained MD simulations were conducted at 1 atm and 300 K under the NPT ensemble condition. During the simulation, the SHAKE algorithm[33] was applied to constrain the covalent bonds to hydrogen atoms. A time step of 2.0 fs and a nonbonding interaction cutoff radius of 10.0 Å were used. Coordinates were saved every 1.0 ps during the entire process.

2.6. Calculation of Volume of the Active Site. The volume of the active site of CYP2A6 as well as its N297S and A481T mutants was estimated using the *Proshape Pocket* program.[34] The program is based on the Alpha Shape theory, which provides an analytic method for detecting pockets in proteins and measuring their volume and surface area. A probe radius of 1.4 Å was employed. Because the program cannot recognize the heme group, we subtracted the volume of heme group (approximately 200 Å^3) from the preliminary calculation results as suggested by the previous work.[35]

2.7. Binding Free Energy Calculations. The binding free energy between coumarin and the protein was calculated with the MM-PBSA approach,[36−38] according to the following equation:

$$\Delta G_{\text{binding}} = \Delta G_{\text{MM}} + \Delta G_{\text{solv}} - T\Delta S \quad (1)$$

where $\Delta G_{\text{binding}}$ is the binding free energy, ΔG_{MM} is the molecular mechanical energy, ΔG_{solv} is the solvation energy, and $T\Delta S$ is the entropy contribution. The molecular mechanical energy is calculated by the following equation:

$$\Delta G_{\text{MM}} = \Delta G_{\text{int}} + \Delta G_{\text{elec}} + \Delta G_{\text{vdw}} \quad (2)$$

where ΔG_{int}, ΔG_{elec}, and ΔG_{vdw} represent internal, electrostatic, and van der Waals energy in the gas phase, respectively. The solvation energy is divided into two components:

$$\Delta G_{\text{solv}} = \Delta G_{\text{ele,sol}} + \Delta G_{\text{nonpol,sol}} \quad (3)$$

where $\Delta G_{\text{ele,sol}}$ is the electrostatic contribution to solvation energy, and $\Delta G_{\text{nonpol,sol}}$ is the nonpolar solvation term. Here, the polar contribution was calculated by solving the Poisson−Boltzmann equation, whereas the latter is determined using,

$$\Delta G_{\text{nonpol,sol}} = \gamma(\text{SASA}) + b \quad (4)$$

where γ represents surface tension and b is constant, whereas SASA is the solvent-accessible surface area (Å^2).

In this study, 200 snapshots from the last 2.0 ns of production stage were extracted for binding free energy calculations. The polar contribution term of solvation energy was calculated using the *PBSA* program in *Amber9*. The interior dielectric constant was set to 1.0, and the outer dielectric constant was set to 80.0. The solvent-accessible surface area was determined using the LCPO method.[39] The coefficient γ and b were set to 0.0072 kcal /(mol·Å^2) and 0 respectively, as in the work of Still and co-workers.[40] Normal mode analysis[41] was conducted to estimate the entropic changes using the nmode program in *Amber9*. Because the current CYP2A6 systems are relatively large (about 8000 atoms excluding water and ions) and thus very memory demanding, only residues within 12.0 Å of the substrate were included for the normal mode calculations. This treatment has been used in many previous studies.[26,42] The truncated systems were minimized for up to 100 000 cycles to give an energy gradient of 0.0001 kcal·mol^{-1}·Å^{-1} using a distance-dependent dielectric constant of $\varepsilon = 4r$. Fifty snapshots of each system were selected for the entropy calculation.

3. Results and Discussion

At present, only the crystal structure of 2A6 WT in complex with coumarin has been determined, and no structural models are available for the N297S and A481T mutant complexes. Therefore, first we need to construct the mutant complexes models. The crystal structure of WT−coumarin complex[17] reveals that the substrate forms a direct hydrogen bond with Asn297, which implies that the replacement of Asn297 by other residues could change the binding orientation of the substrate in the active site of the enzyme. In addition, previous studies on other CYPs indicated that a single residual mutation could indeed result in different binding orientations of the ligand in the active site of the enzymes.[43,44] Bearing these facts in mind, we adopted the following protocol to investigate the effect of two mutations on the catalytic activity of CYP2A6. First, we constructed the protein models of substrate-free mutants based on the crystal structure of WT−coumarin complex. Then, the initial complex models of mutants were built by docking coumarin into the active site of substrate-free mutant models. After that, long-time MD simulations of the WT and mutant complexes were performed to refine the substrate binding modes and explore the dynamic behaviors of proteins and the substrate in the active site of the enzymes. Finally, binding free energy was calculated to analyze the energy differences between WT and the mutants.

3.1. Models of N297S and A481T Mutant Proteins. The protein models of substrate-free N297S and A481T mutants were obtained by a 1.0 ns MD simulation and then energy-minimization. For comparison, the substrate-free WT was also built using the same procedure as the mutant construction. The root-mean-square deviations (rmsd) of backbone atoms of N297S and A481T with respect to WT were 0.20 Å and 0.18 Å, respectively. Comparison of the mutant models with WT revealed that only a few residues adjacent to the mutated residues underwent slight displacement, primarily for the phenylalanine residues in the Phe-cluster. In the N297S mutant, Ser297 formed a stable hydrogen bond via the side-chain hydroxyl group with the backbone oxygen atom of its neighboring residue Met293. The phenyl ring of Phe111 in the N297S mutant had a slight rotation compared to WT. The same event has been observed in the crystal structures of other substrate-free CYP2A6 mutants including N297Q, N297Q/L241C, and N297Q/I300V.[18] All of these mutants exhibit no significant backbone changes but slight displacement in side chains of certain residues in the active sites. For the A481T mutant, the side chains of Phe209 and Phe480 underwent a slight displacement when compared to WT. Both residues are situated around the mutated Thr481.

3.2. Complex Models of N297S and A481T with Coumarin by Docking. The initial complex models of N297S and A481T with coumarin were obtained by using the docking program *GOLD*. Prior to obtaining the mutant complexes using *GOLD*, the binding mode of WT with coumarin was reproduced by docking the substrate into the MD-refined substrate-free WT model. The docking result showed that coumarin displayed similar binding orientation to that of the crystal structure of WT−coumarin except a slight translation of the planar ring of coumarin. This is not surprising because coumarin is planar and small in size. For consistency, the comparison of the mutant complexes with respect to WT was based on the docked WT−coumarin complex model.

Compared with the WT−coumarin complex, the binding mode of coumarin in the active site of N297S differed significantly (Figure S1 of the Supporting Information). Because Ser297 formed a hydrogen bond with Met293, no hydrogen bond between Ser297 and coumarin was observed.

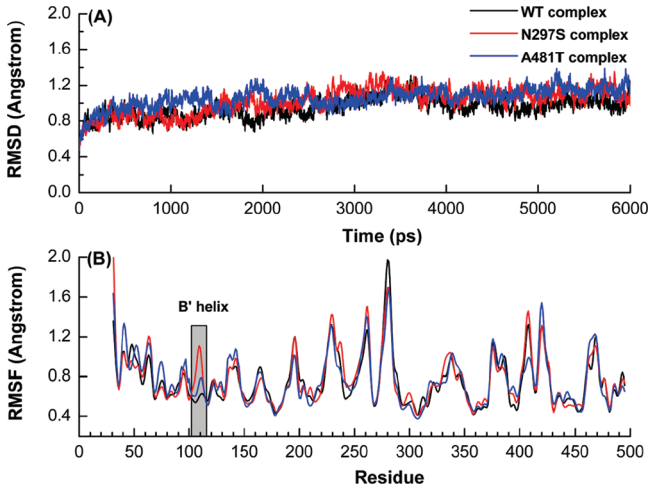

Figure 2. (A) rmsd variations of CYP2A6 WT (black), N297S (red), and A481T (blue) mutants with respect to the starting structures as a function of simulation time. (B) RMSF of non-hydrogen atoms versus residue position of WT (black), the N297S mutant (red), and the A481T mutant (blue) calculated from MD simulations. The shadow region represents the B′ helix.

Although coumarin kept a binding pose similar to that in the WT complex, the planar ring had an obvious deviation in the N297S complex. Because the hydrogen bond is abolished and thus the altered binding mode, the Chemscore of coumarin with N297S (27.4) was lower than that of coumarin with WT (29.2). In contrast, the binding mode of coumarin in the A481T mutant was almost the same as that of the WT complex. A direct hydrogen bond was formed between Asn297 and coumarin in the A418T complex. Because Asn297 is the only polar residue in the active site of CYP2A6 and the side chain is pointing to the active site, this residue easily guides the binding orientation of the substrates that have hydrogen-bonding acceptors. The docking score was 28.9 for coumarin with A481T. Neither the substrate binding modes nor the docking scores can differentiate the interactions between WT and A481T with coumarin. Several recent studies[45,46] clearly demonstrated that automated docking alone was not suitable for accurate discrimination of the ligands and/or proteins that have structurally high similarity. However, docking combined with MD simulations was shown to successfully achieve the goal. Therefore, the 2A6 WT and the mutant complexes were subsequently subjected to 6 ns unrestrained MD simulations.

3.3. MD Simulations of 2A6 Complexes. MD simulations were performed on each complex with two purposes. The first is to refine the substrate binding modes because the docking does not take into account the flexibility of proteins. The other purpose is to explore the dynamic behavior of the proteins and the substrate in the active site of the enzymes during the long-time MD simulations.

Overall Structural Changes. The rmsd values of protein backbone atoms with the individual starting structure were monitored along the whole MD process. Part A of Figure 2 shows the rmsd of three systems as they vary with respect to simulation time. The rmsd values of three complexes have a large fluctuation during the first 4.0 ns and reach stability after 4.0 ns. The protein atoms do not undergo significant structural changes and the rmsd values of the three systems converge to about 1.1 Å, a relatively small deviation from the minimized structure. Because the rmsd values showed no significant fluctuation after 4.0 ns in all three systems, subsequent analysis was performed on the snapshots from the last 2.0 ns.

To examine the mobility of protein residues, the root-mean-square fluctuation (RMSF) of backbone atoms of each residue was investigated, as shown in part B of Figure 2. The three structures have similar profiles in RMSF distribution except for the shadow region, which represents the B′ helix. This region displays relatively large RMSF values in the N297S mutant. This mainly attributes to the N297S mutation, which altered the interactions between this region and the I helix, as discussed in the following section. Apart from the N-terminus, residues with the large RMSF value belong to the loops connected with two well-conserved secondary structures, α helices, or β sheets. Because these loops are located at the surface of the protein and completely exposed to the solvent, it is not surprising that these regions have a large RMSF. This trend of RMSF calculated by our simulations is also in accordance with deduction from the crystal structure.[17]

Conformational Change of Residues in the Active Site. To address the structural difference between WT and the mutants during the long-time MD simulations, we analyzed the conformational changes of residues in the active sites. The average structures of three complexes were first calculated with 200 snapshots, which were extracted from the last 2.0 ns. Then, the average structures of the N297S and A481T mutants were superimposed on that of WT with protein backbone atoms. The superposition demonstrates that these three protein structures are similar in whole. The rmsd value of the N297S mutant with WT is 0.84 Å and it is 0.95 Å between the A481T mutant and WT. However, detailed analysis of the individual residues at the active site and comparison of local structures provide new insights into the structural changes due to mutations.

Comparison of the N297S mutant with WT revealed a movement of the B′−C loop involving residues Val116-Ser119, and a slight outward shift of the B′ helix occurred in the N297S mutant, as shown in part A of Figure 3. Several Phe residues of the Phe-cluster in the N297S mutant, such as Phe107, Phe111, and Phe118, underwent displacement when compared to WT. The shift of the B′ helix/B′−C loop region resulted in an expansion of the active site and thus an enlargement in the volume of the active site of the N297S mutant. To confirm this view, we estimated the volumes of active sites of WT and the N297S mutant. As expected, the average volumes of those of WT and the N297S mutant are 147 Å^3 and 167 Å^3, respectively. The active site volume of the N297S mutant is about 14% larger than that of WT. The calculated volumes are comparable to the values calculated by another group using the same program.[35]

Detailed analysis of the MD trajectories of N297S and WT indicated that the shift of the B′ helix/B′−C loop region was primarily caused by the change of the hydrogen-bonding network around residue 297. The crystal structure of WT complexed with coumarin[17] reveals that Asn297 interacts

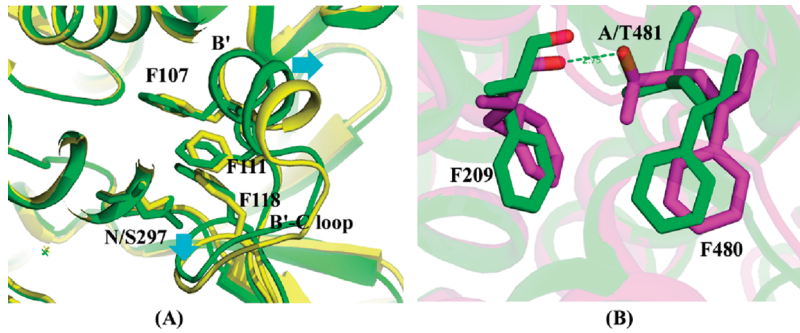

Figure 3. Superposition of average structures from the last 2 ns of the three complexes. (A) Superposition between WT (green) and the N297S mutant (yellow). (B) Superposition between WT (green) and the A481T mutant (magenta). Important secondary structure elements and the residues with significant structural changes are labeled. The arrow indicates the movement of the secondary elements.

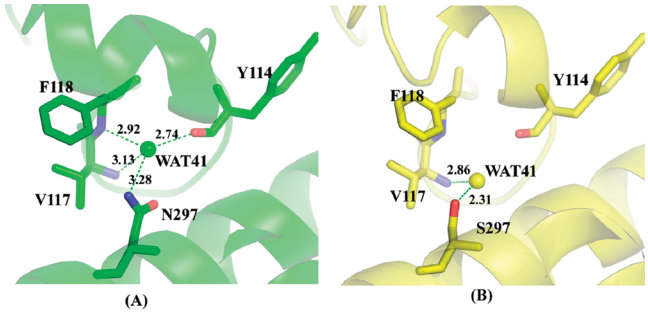

Figure 4. Hydrogen bonding network mediated by WAT41 in MD snapshots of (A) the WT complex and (B) the N297S complex. Hydrogen bonds are represented by the green dotted lines and the distances (Å) between heavy atoms are labeled.

with the B′−C loop via a water molecule (WAT41) mediation. The water molecule forms hydrogen bonds with the backbone N atoms of both Val117 and Phe118, the backbone O atom of Tyr114, and the side chain N atom of Asn297. During the MD simulation of the WT complex, the water molecule kept the hydrogen-bonding network interactions the same as those of the crystal structure. WAT41 formed hydrogen bonds with Asn297, Val117, Phe118, and Tyr114, as shown in part A of Figure 4. The occupancy of these hydrogen bonds is greater than 50% of the last 2.0 ns MD simulation, as shown in Table 1. In contrast, the hydrogen-bonding network mediated by WAT41 in the N297S mutant was changed due to the shortened side chain of Ser297. In the N297S mutant, WAT41 maintained hydrogen-bonding interactions with more than 50% occupancy only with Val117 and Ser297 (part B of Figure 4). The hydrogen-bonding network formed by WAT41 in the A481T mutant was similar to that of WT (Table 1). Because the B′ helix/B′−C loop region directly interacts with the I helix and constitutes a part of the substrate binding pocket, the region was considered to play an essential role in the substrate binding.[18] Previous mutagenesis experiments confirmed that residues in the B′ helix/B′−C loop region affected the catalytic activity of CYP2B1.[47]

In addition to the shift of the B′ helix/B′−C loop region, the phenyl ring of Phe111 in the N297S mutant underwent a rotation compared to WT. To identify the ring rotation, the change of the side-chain torsion χ_2 (CA, CB, CG, and CD1) of Phe111 was monitored for the WT and N297S complexes, as shown in part A of Figure 5. Compared to WT, the torsion angle of Phe111 in the N297S mutant has an obvious change. Phe111 is located above the residue 297 and has hydrophobic interactions with residue 297. The substitution of Asn by Ser at position 297 leads to a shorter side chain and thus changes the interaction with Phe111. This may be the reason for rotation of the Phe111 ring. The rotation of the phenyl ring of Phe111 due to the change of residue 297 has been observed in the crystal structures of CYP2A6 and in other mutants including N297Q and N297Q/L240C.[18]

The crystal structure of 2A6 bound with coumarin[17] reveals that Ala481 is a distance of about 7.6 Å from the substrate and does not directly interact with coumarin. Accordingly, the A481T mutation may influence the substrate binding through an indirect manner, that is, the mutation affects its neighboring residues to transfer the effect. This

Table 1. Hydrogen Bonding Networks Mediated by WAT41 During the Last 2 ns of MD Simualtions

Donor		Acceptor		Occupancy (%)
		WT		
Phe118	H	O	WAT41	97.3
Val117	H	O	WAT41	86.5
Asn297	HD21	O	WAT41	75.5
WAT41	H1	O	Tyr114	58.2
WAT41	H2	O	Tyr114	53.4
WAT41	H1	N	Phe118	24.1
WAT41	H2	N	Phe118	19.9
WAT41	H1	ND2	Asn297	17.8
WAT41	H2	ND2	Asn297	15.6
		N297S		
Val117	H	O	WAT41	99.8
WAT41	H1	OG	Ser297	50.5
WAT41	H2	OG	Ser297	50.1
WAT41	H1	O	Tyr114	26.6
WAT41	H2	O	Tyr114	24.7
		A481T		
Phe118	H	O	WAT41	96.7
Val117	H	O	WAT41	77.5
Asn297	HD21	O	WAT41	74.5
WAT41	H1	O	Tyr114	57.0
WAT41	H2	O	Tyr114	57.6
WAT41	H1	N	Phe118	18.1
WAT41	H2	N	Phe118	16.2
WAT41	H1	ND2	Asn297	16.7
WAT41	H2	ND2	Asn297	15.3

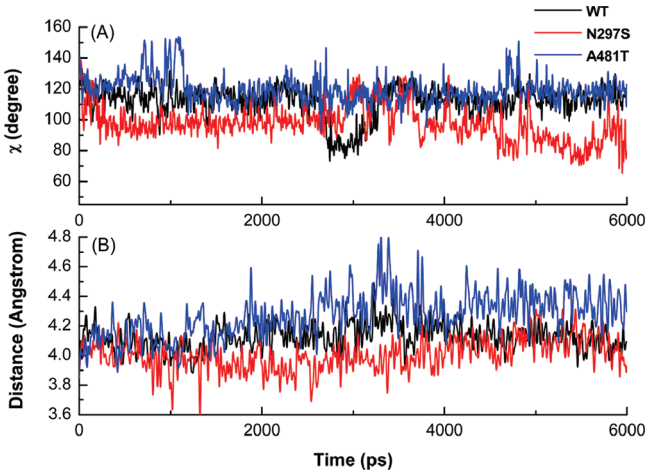

Figure 5. (A) Variation of the side-chain torsion χ_2 (CA, CB, CG, and CD1) of Phe111 in three complexes versus time. (B) The variation of distances between Fe and C-7 of coumarin versus simulation time.

idea was supported by our modeling and MD simulations. Superimposition of WT with the A481T mutant indicated the mutation caused significant displacement of Phe480 and an altered orientation of Phe209 when compared with WT, as shown in part B of Figure 3. Both residues belong to the Phe-cluster mention earlier.

Although the replacement of Ala481 by Thr increases the length and size of residue 481, Thr481 still cannot directly make contact with the substrate. Nevertheless, the mutated Thr481 side chain was enough to trigger the structural changes of its adjacent residues. To accommodate the increased size of residue 481, the phenyl ring of Phe480 moved away from Thr481 by about 1.5 Å relative to WT. On the other hand, the hydroxyl group of the side chain of Thr481 formed a hydrogen bond with the backbone oxygen atom of Phe209. The direct interaction makes the contact between these two residues more intimate. This may be one of the reasons that the orientation of Phe209 was changed in the A481T mutant. Both Phe480 and Phe209 have been demonstrated to substantially alter the catalytic activity of 2A6[14] and other 2A enzymes[48] when the Phe residue at positions 480 or 209 was replaced by other residues. Because both affected residues, Phe480 and Phe209, move away from the active site, the synchronous effect of these residues' movement resulted in the expansion of the volume of the active site in the A481T mutant. The calculated average volume of the active site of the A481T mutant is approximately 177 Å^3, roughly a 20% increase from that of WT.

Substrate Binding Mode. The influence of mutation on the binding modes of coumarin in the active site was investigated

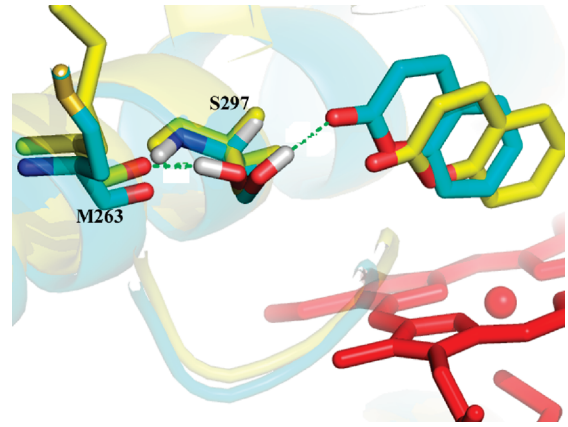

Figure 6. Substrate induced the side-chain conformational change of Ser297 in the N297S mutant during MD simulation. Yellow, before MD simulation; cyan, after MD refinement.

by analyzing the MD trajectories. Superimposition of the average structures of the substrate demonstrated that neither mutation significantly altered the substrate binding modes. Although the active-site volume of the A481T mutant is about 20% larger than that of WT, the alteration did not induce the change in the substrate binding. This mainly contributes to the facts that the active site of CYP2A6 is highly hydrophobic and tightly packed and that only polar residue 297 in the active site provides a hydrogen-bonding donor so as to orient coumarin binding.

Interestingly, the substrate induced a rotation of the side chain of Ser297 during the MD simulation of the N297S mutant. Before MD simulation, the hydroxyl group of Ser297 pointed to Met293 and formed a hydrogen bond with the backbone oxygen atom of Met293. After MD refinement, however, the hydroxyl group pointed to coumarin and formed a hydrogen bond with the oxygen atom of the substrate, as shown in Figure 6. The induced-fit phenomenon caused by ligand binding has been observed in the crystal structures of several P450s, notably CYP2C9 and CYP2B4, for instance. The trivial difference of binding modes between N297S and WT is in agreement with the experimental data. Previous studies indicated that the N297S mutation did not affect the K_{cat} value but only decreased the K_m by about 4-fold for coumarin 7-hydroxylation.[16]

Although similar substrate binding orientations were observed for the A481T mutant and WT, the distances of C-7 of coumarin from the iron atom differed in these two enzymes. Part B of Figure 5 shows the distance variation of C-7 and Fe along the MD simulations of three systems. The distance of C-7 and Fe in the N297S mutant is almost same as that of WT. In contrast, the average distance of C-7 and Fe in the A481T mutant is 0.3 Å longer than that of WT. It

Table 2. Binding Free Energies of P450 2A6 WT, N297S, and A481T Complexed with Coumarin[a]

2A6	ΔG_{ele}	ΔG_{vdw}	$\Delta G_{nonp,sol}$	$\Delta G_{ele,sol}$	$-T\Delta S$	$\Delta G^{cal}_{binding}$	$\Delta G^{exp}_{binding}$ [b]	$\Delta G^{exp}_{binding}$ [c]
WT	−12.20 ± 0.12	−25.45 ± 0.09	−2.90 ± 0.01	20.40 ± 0.08	12.37 ± 0.54	−7.78	−8.19	−7.80
N297S	−14.36 ± 0.13	−23.53 ± 0.10	−3.03 ± 0.01	23.13 ± 0.06	11.76 ± 0.56	−6.03	−6.19	−7.02
A481T	−11.75 ± 0.07	−24.78 ± 0.09	−3.05 ± 0.01	21.45 ± 0.08	12.31 ± 0.56	−5.82	−6.17	−6.99

[a] All energies are in kcal/mol. The uncertainties are the standard error of the mean calculated with 200 snapshots (50 snapshots for entropic calculations). [b] $\Delta G^{exp}_{binding}$: calculated from the experimental data via $\Delta G^{exp}_{binding} \approx RT \ln K$ at $T = 300$ K. The binding energies are calculated based on K_s. [c] The binding energies are calculated based on K_m.

is well-known that the distance between the oxidation distance and Fe can influence the activation energy of the proton and electron transfer reaction.[49] The increase of the distance may lead to a decrease in the reaction rate. This may account for the experimental result that the K_{cat} value of A481T decreases ~3-fold toward coumarin 7-hydroxylation as compared with WT. A previous study also reported a similar finding for CYP2A6 V117A mutation with coumarin 7-hydroxylation.[50]

3.4. Binding Free Energy Analysis. Binding free energies of WT and the mutants were calculated and analyzed with the MM-PBSA method. Table 2 lists the calculated energies, including the total binding energies and the individual energy components. According to Table 2, the WT complex has the lowest binding energy. Binding energies of both mutants are higher than that of WT. The recent biochemical experiment indicated that the K_s and K_m values of both mutants with coumarin were higher than that of WT.[16] Generally, the greater the K_s or K_m value is, the lower binding affinity the enzyme has for substrates. It is encouraging that our predicted binding energies are in good agreement with the relative potency of the experimental binding affinities.

A detailed energy analysis showed that van der Waals energies are the major driving force for the substrate−enzyme binding. This is in line with the fact that the active site of CYP2A6 is mainly composed of hydrophobic residues. Compared to WT, the van der Waals energy shows a considerable increase in the N297S mutant. This was mainly caused by the shift of the B′ helix/B′−C loop region due to the N297S mutation. The electrostatic interaction energy of N297S was more favorable for the substrate binding than that of WT. However, the solvation electrostatic energy and the van der Waals energy canceled the favorable contribution. For the A481T mutant, the difference was not so significant because the mutation affected the substrate binding via an indirect manner. However, the accumulation of the energy differences made the substrate binding unfavorable with the A481T mutant.

4. Conclusions

Molecular docking combined with MD simulations and binding energy calculations was performed on human CYP2A6 as well as its N297S and A481T mutants complexed with coumarin for the purpose of elucidating the mechanisms underlying the reduced catalytic activity and binding affinity due to residual mutations. Our simulations demonstrated that the N297S mutation caused an altered hydrogen-bonding network mediated by a water molecule between the B′−C loop and the I helix and thus a shift of the B′ helix/B′−C loop region, whereas the A481 mutation triggered the conformation changes of its adjacent residues including Phe209 and Phe480 via an indirect manner to affect the substrate binding. Neither mutation significantly changed the substrate binding orientations but did distort the shape of the Phe-cluster in the active site and thus weakened the interactions with coumarin. In addition, very interestingly, the N297S mutation induced a conformation rotation of the side chain of Ser297 during MD simulations. The calculated binding free energies were in good agreement with the relative potency of the experimental binding affinities. To verify our results, which are based on molecule A, molecule B in the crystal structure of 1Z10 was also used to perform the modeling and MD simulations using the same procedure as that of molecule A. A similar protein and substrate dynamic behavior occurred as presented here. Part of the results based on molecule B was provided in the Supporting Information. Our findings will be very useful for understanding the biological function of CYP2A6.

Acknowledgment. We thank Dr. Danni L. Harris for his kindness in offering us the heme parameters. The author (W. Li) thanks the Japanese Society for the Promotion of Science (JSPS) research fellowship for foreign researchers. This work was supported by the Grant-in-Aid for Scientific Research from JSPS. The author (Y. Tang) also gratefully acknowledges financial support from National Natural Science Foundation of China (Grants 20572023).

Supporting Information Available: Part of the results based on molecule B of the crystal structure of the WT-coumarin complex was presented in the supporting material. This material is available free of charge via the Internet at http://pubs.acs.org.

References

(1) Rendic, S. Summary of information on human CYP enzymes: Human P450 metabolism data. *Drug Metab. Rev.* **2002**, *34*, 83–448.

(2) Guengerich, F. P. Human Cytochrome P450 enzymes. In *Cytochrome P450:Strucuture, Mechanism, and Biochemistry*, 3rd ed.; Ortiz de Montellano, R. R., Ed.; Klumer Academic/Plenum Publishers: New York, 2005; pp 377−531.

(3) Yun, C. H.; Shimada, T.; Guengerich, F. P. Purification and characterization of human liver microsomal cytochrome P-450 2A6. *Mol. Pharmacol.* **1991**, *40*, 679–685.

(4) Pelkonen, O.; Rautio, A.; Raunio, H.; Pasanen, M. CYP2A6: a human coumarin 7-hydroxylase. *Toxicology* **2000**, *144*, 139–147.

(5) Cashman, J. R.; Park, S. B.; Yang, Z. C.; Wrighton, S. A.; Jacob, P., 3rd; Benowitz, N. L. Metabolism of nicotine by human liver microsomes: Stereoselective formation of *trans*-nicotine *N*′-oxide. *Chem. Res. Toxicol.* **1992**, *5*, 639–646.

(6) Idle, J. R. CYP2A6 polymorphism, nicotine, and environmental nitrosamines. *Lancet* **1999**, *353*, 2073.

(7) Yamazaki, H.; Inui, Y.; Yun, C. H.; Guengerich, F. P.; Shimada, T. Cytochrome P450 2E1 and 2A6 enzymes as major catalysts for metabolic activation of *N*-nitrosodialkylamines and tobacco-related nitrosamines in human liver microsomes. *Carcinogenesis* **1992**, *13*, 1789–1794.

(8) Oscarson, M.; Gullsten, H.; Rautio, A.; Bernal, M. L.; Sinues, B.; Dahl, M. L.; Stengard, J. H.; Pelkonen, O.; Raunio, H.; Ingelman-Sundberg, M. Genotyping of human cytochrome P450 2A6 (CYP2A6), a nicotine C-oxidase. *FEBS Lett.* **1998**, *438*, 201–205.

(9) Yano, J. K.; Denton, T. T.; Cerny, M. A.; Zhang, X. D.; Johnson, E. F.; Cashman, J. R. Synthetic inhibitors of cytochrome P-450 2A6: Inhibitory activity, difference spectra, mechanism of inhibition, and protein cocrystallization. *J. Med. Chem.* **2006**, *49*, 6987–7001.

(10) Ikeda, K.; Yoshisue, K.; Matsushima, E.; Nagayama, S.; Kobayashi, K.; Tyson, C. A.; Chiba, K.; Kawaguchi, Y. Bioactivation of tegafur to 5-fluorouracil is catalyzed by cytochrome P-450 2A6 in human liver microsomes in vitro. *Clin. Cancer Res.* **2000**, *6*, 4409–4415.

(11) Torchin, C. D.; McNeilly, P. J.; Kapetanovic, I. M.; Strong, J. M.; Kupferberg, H. J. Stereoselective metabolism of a new anticonvulsant drug candidate, losigamone, by human liver microsomes. *Drug Metab. Dispos.* **1996**, *24*, 1002–1008.

(12) Rautio, A. Polymorphic CYP2A6 and its clinical and toxicological significance. *Pharmacogen. J* **2003**, *3*, 5–7.

(13) Gillam, E. M.; Aguinaldo, A. M.; Notley, L. M.; Kim, D.; Mundkowski, R. G.; Volkov, A. A.; Arnold, F. H.; Soucek, P.; DeVoss, J. J.; Guengerich, F. P. Formation of indigo by recombinant mammalian cytochrome P450. *Biochem. Biophys. Res. Commun.* **1999**, *265*, 469–472.

(14) Nakamura, K.; Martin, M. V.; Guengerich, F. P. Random mutagenesis of human cytochrome p450 2A6 and screening with indole oxidation products. *Arch. Biochem. Biophys.* **2001**, *395*, 25–31.

(15) Guengerich, F. P.; Sorrells, J. L.; Schmitt, S.; Krauser, J. A.; Aryal, P.; Meijer, L. Generation of new protein kinase inhibitors utilizing cytochrome p450 mutant enzymes for indigoid synthesis. *J. Med. Chem.* **2004**, *47*, 3236–3241.

(16) Kim, D.; Wu, Z. L.; Guengerich, F. P. Analysis of coumarin 7-hydroxylation activity of cytochrome P450 2A6 using random mutagenesis. *J. Biol. Chem.* **2005**, *280*, 40319–40327.

(17) Yano, J. K.; Hsu, M. H.; Griffin, K. J.; Stout, C. D.; Johnson, E. F. Structures of human microsomal cytochrome P450 2A6 complexed with coumarin and methoxsalen. *Nat. Struct. Mol. Biol.* **2005**, *12*, 822–823.

(18) Sansen, S.; Hsu, M. H.; Stout, C. D.; Johnson, E. F. Structural insight into the altered substrate specificity of human cytochrome P450 2A6 mutants. *Arch. Biochem. Biophys.* **2007**, *464*, 197–206.

(19) Jones, G.; Willett, P.; Glen, R. C.; Leach, A. R.; Taylor, R. Development and validation of a genetic algorithm for flexible docking. *J. Mol. Biol.* **1997**, *267*, 727–748.

(20) Kirton, S. B.; Murray, C. W.; Verdonk, M. L.; Taylor, R. D. Prediction of binding modes for ligands in the cytochromes P450 and other heme-containing proteins. *Proteins* **2005**, *58*, 836–844.

(21) Hritz, J.; de Ruiter, A.; Oostenbrink, C. Impact of Plasticity and Flexibility on Docking Results for Cytochrome P450 2D6: A Combined Approach of Molecular Dynamics and Ligand Docking. *J. Med. Chem.* **2008**, *51*, 7469–7477.

(22) Guengerich, F. P. Common and uncommon cytochrome P450 reactions related to metabolism and chemical toxicity. *Chem. Res. Toxicol.* **2001**, *14*, 611–650.

(23) Becke, A. D. Density-functional thermochemistry. III. The role of exact exchange. *J. Chem. Phys.* **1993**, *98*, 5648–5652.

(24) Lee, C.; Yang, W.; Parr, R. G. Development of the Colle-Salvetti correlation-energy formula into a functional of the electron density. *Phys. Rev. B* **1988**, *37*, 785–789.

(25) Gilson, M. K.; Sharp, K. A.; Honig, B. H. Calculating the electrostatic potential of molecules in solution. *J. Comput. Chem.* **1988**, *9*, 327–335.

(26) Harris, D. L.; Park, J. Y.; Gruenke, L.; Waskell, L. Theoretical study of the ligand-CYP2B4 complexes: Effect of structure on binding free energies and heme spin state. *Proteins* **2004**, *55*, 895–914.

(27) Frisch, M. J. T., G. W.; Schlegel, H. B.; Scuseria, G. E.; Robb, M. A.; Cheeseman, J. R.; Montgomery, J. A., Jr.; Vreven, T.; Kudin, K. N.; Burant, J. C.; Millam, J. M.; Iyengar, S. S.; Tomasi, J.; Barone, V.; Mennucci, B.; Cossi, M.; Scalmani, G.; Rega, N.; Petersson, G. A.; Nakatsuji, H.; Hada, M.; Ehara, M.; Toyota, K.; Fukuda, R.; Hasegawa, J.; Ishida, M.; Nakajima, T.; Honda, Y.; Kitao, O.; Nakai, H.; Klene, M.; Li, X.; Knox, J. E.; Hratchian, H. P.; Cross, J. B.; Bakken, V.; Adamo, C.; Jaramillo, J.; Gomperts, R.; Stratmann, R. E.; Yazyev, O.; Austin, A. J.; Cammi, R.; Pomelli, C.; Ochterski, J. W.; Ayala, P. Y.; Morokuma, K.; Voth, G. A.; Salvador, P.; Dannenberg, J. J.; Zakrzewski, V. G.; Dapprich, S.; Daniels, A. D.; Strain, M. C.; Farkas, O.; Malick, D. K.; Rabuck, A. D.; Raghavachari, K.; Foresman, J. B.; Ortiz, J. V.; Cui, Q.; Baboul, A. G.; Clifford, S.; Cioslowski, J.; Stefanov, B. B.; Liu, G.; Liashenko, A.; Piskorz, P.; Komaromi, I.; Martin, R. L.; Fox, D. J.; Keith, T.; Al-Laham, M. A.; Peng, C. Y.; Nanayakkara, A.; Challacombe, M.; Gill, P. M. W.; Johnson, B.; Chen, W.; Wong, M. W.; Gonzalez, C.; Pople, J. A. *Gaussian 03*; Gaussian, Inc.: Wallingford, CT, 2004.

(28) Hui, Li; Robertson, A. D.; Jensen, J. H. Very fast empirical prediction and interpretation of protein pK_a values. *Proteins* **2005**, *61*, 704–721.

(29) Case, D. A.; Cheatham, T. E., 3rd; Darden, T.; Gohlke, H.; Luo, R.; Merz, K. M., Jr.; Onufriev, A.; Simmerling, C.; Wang, B.; Woods, R. J. The Amber biomolecular simulation programs. *J. Comput. Chem.* **2005**, *26*, 1668–1688.

(30) Jorgensen, W. L.; Chandrasekhar, J.; Madura, J.; Klein, M. L. Comparison of simple potential functions for simulating liquid water. *J. Chem. Phys.* **1983**, *79*, 926–935.

(31) Duan, Y.; Wu, C.; Chowdhury, S.; Lee, M. C.; Xiong, G. M.; Zhang, W.; Yang, R.; Cieplak, P.; Luo, R.; Lee, T.; Caldwell, J.; Wang, J. M.; Kollman, P. A point-charge force field for molecular mechanics simulations of proteins based on condensed-phase quantum mechanical calculations. *J. Comput. Chem.* **2003**, *24*, 1999–2012.

(32) Wang, J.; Wolf, R. M.; Caldwell, J. W.; Kollman, P. A.; Case, D. A. Development and testing of a general amber force field. *J. Comput. Chem.* **2004**, *25*, 1157–1174.

(33) Rychaert, J. P.; Ciccotti, G.; Berendsen, H. J. C. Numerical integration of the cartesian equations of motion of a system with constraints: Molecular dynamics of n-alkanes. *J. Comput. Phys.* **1977**, *23*, 327–341.

(34) Liang, J.; Edelsbrunner, H.; Woodward, C. Anatomy of protein pockets and cavities:measurement of binding site geometry and implications for ligand design. *Protein Sci.* **1998**, *7*, 1884–1897.

(35) Rydberg, P.; Rod, T. H.; Olsen, L.; Ryde, U. Dynamics of water molecules in the active-site cavity of human cytochromes P450. *J. Phys. Chem. B* **2007**, *111*, 5445–5457.

(36) Massova, I.; Kollman, P. A. Combined molecular mechanical and continuum solvent approach (MM-PBSA/GBSA) to predict ligand binding. *Perspect. Drug Discov. Des.* **2000**, *18*, 113–135.

(37) Wang, J. M.; Morin, P.; Wang, W.; Kollman, P. A. Use of MM-PBSA in reproducing the binding free energies to HIV-1 RT of TIBO derivatives and predicting the binding mode to HIV-1 RT of efavirenz by docking and MM-PBSA. *J. Am. Chem. Soc.* **2001**, *123*, 5221–5230.

(38) Kollman, P. A.; Massova, I.; Reyes, C.; Kuhn, B.; Huo, S. H.; Chong, L.; Lee, M.; Lee, T.; Duan, Y.; Wang, W.; Donini, O.; Cieplak, P.; Srinivasan, J.; Case, D. A.; Cheatham, T. E. Calculating structures and free energies of complex molecules:

Combining molecular mechanics and continuum models. *Acc. Chem. Res.* **2000**, *33*, 889–897.

(39) Weiser, J.; Shenkin, P. S.; Still, W. C. Approximate atomic surfaces from linear combinations of pairwise overlaps (LCPO). *J. Comput. Chem.* **1999**, *20*, 217–230.

(40) Still, W. C.; Tempczyk, A.; Hawley, R. C.; hendrickson, T. Semianalytical treatment of solvation for molecular mechanics and dynamics. *J. Am. Chem. Soc.* **1990**, *112*, 6127–6129.

(41) Brooks, B. R.; Janezic, D.; Karplus, M. Harmonic analyis of large systems. *J. Comput. Chem.* **1995**, *16*, 1522–1553.

(42) Weis, A.; Katebzadeh, K.; Soderhjelm, P.; Nilsson, I.; Ryde, U. Ligand affinities predicted with the MM/PBSA method: dependence on the simulation method and the force field. *J. Med. Chem.* **2006**, *49*, 6596–6606.

(43) Feenstra, K. A.; Starikov, E. B.; Urlacher, V. B.; Commandeur, J. N.; Vermeulen, N. P. Combining substrate dynamics, binding statistics, and energy barriers to rationalize regioselective hydroxylation of octane and lauric acid by CYP102A1 and mutants. *Protein Sci.* **2007**, *16*, 420–431.

(44) de Graaf, C.; Oostenbrink, C.; Keizers, P. H.; van Vugt-Lussenburg, B. M.; Commandeur, J. N.; Vermeulen, N. P. Free energies of binding of *R*- and *S*-propranolol to wild-type and F483A mutant cytochrome P450 2D6 from molecular dynamics simulations. *Eur. Biophys. J.* **2007**, *36*, 589–599.

(45) de Graaf, C.; Oostenbrink, C.; Keizers, P. H.; van der Wijst, T.; Jongejan, A.; Vermeulen, N. P. Catalytic site prediction and virtual screening of cytochrome P450 2D6 substrates by consideration of water and rescoring in automated docking. *J. Med. Chem.* **2006**, *49*, 2417–2430.

(46) Carlsson, J.; Boukharta, L.; Aqvist, J. Combining docking, molecular dynamics and the linear interaction energy method to predict binding modes and affinities for non-nucleoside inhibitors to HIV-1 reverse transcriptase. *J. Med. Chem.* **2008**, *51*, 2648–2656.

(47) Honma, W.; Li, W.; Liu, H.; Scott, E. E.; Halpert, J. R. Functional role of residues in the helix B' region of cytochrome P450 2B1. *Arch. Biochem. Biophys.* **2005**, *435*, 157–165.

(48) Negishi, M.; Uno, T.; Honkakoski, P.; Sueyoshi, T.; Darden, T. A.; Pedersen, L. P. The roles of individual amino acids in altering substrate specificity of the P450 2a4/2a5 enzymes. *Biochimie* **1996**, *78*, 685–694.

(49) Hata, M.; Tanaka, Y.; Kyoda, N.; Osakabe, T.; Yuki, H.; Ishii, I.; Kitada, M.; Neya, S.; Hoshino, T. An epoxidation mechanism of carbamazepine by CYP3A4. *Bioorg. Med. Chem.* **2008**, *16*, 5134–5148.

(50) He, X. Y.; Shen, J.; Hu, W. Y.; Ding, X.; Lu, A. Y.; Hong, J. Y. Identification of Val117 and Arg372 as critical amino acid residues for the activity difference between human CYP2A6 and CYP2A13 in coumarin 7-hydroxylation. *Arch. Biochem. Biophys.* **2004**, *427*, 143–153.

CT900018T